analytical chemistry

pubs.acs.org/ac Article

Ratiometric Electrochemical Switch for Circulating Tumor DNA through Recycling Activation of Blocked DNAzymes

Hua Chai, Yuguo Tang, Zhenzhen Guo, and Peng Miao*

Cite This: *Anal. Chem.* 2022, 94, 2779−2784 Read Online

ACCESS | Metrics & More | Article Recommendations | Supporting Information

ABSTRACT: Circulating tumor DNA (ctDNA) serves as a powerful noninvasive and viable biomarker for the diagnosis of cancers. The abundance of ctDNA in patients with advanced stages is significantly higher than that in patients with early stages. Herein, a ratiometric electrochemical biosensor for the detection of ctDNA is developed by smart design of DNA probes and recycles of DNAzyme activation. The conformational variation of DNA structures leads to the changes of two types of electrochemical species. This enzyme-free sensing strategy promotes excellent amplification efficiency upon target recognition. The obtained results assure good analytical performances and a limit of detection as low as 25 aM is achieved. Additionally, this method exhibits outstanding selectivity and great application prospects in biological sample analysis.

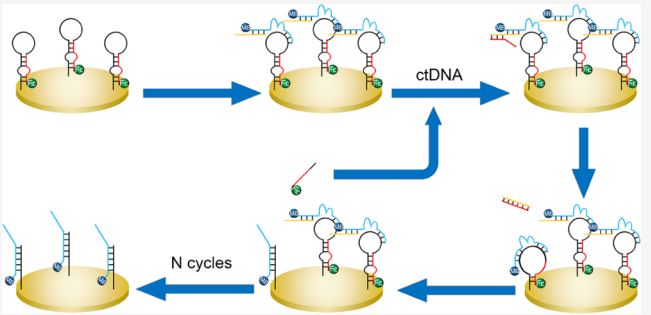

Circulating tumor DNA (ctDNA) belongs to a subset of cell-free small genomic fragments, which originates from tumor cells in the bloodstream.[1,2] ctDNA is an important liquid biopsy biomarker since it carries tumor-specific genetic and epigenetic aberrations.[3] Since ctDNA can be easily found in blood, it shows great potential compared with other traditional invasive biomarkers.[4] However, the abundance of ctDNA is quite low (usually a pico-to-femtomolar level) and the half-life is short (15−150 min) in biological fluids.[5] Therefore, there is an urgent need to develop fast, convenient, and sensitive methods for the detection of ctDNA.[6,7]

At present, a number of techniques have been developed including colorimetry, electrochemistry, fluorescence, electrochemiluminescence (ECL), surface-enhanced Raman scattering (SERS), droplet digital PCR, and so on.[8−12] In these methods, electrochemistry has attracted extensive attention with the advantages of high sensitivity, convenient operation, and ease of miniaturization.[13,14] However, like other techniques, fast response and high sensitivity are usually contradictory since a more complete reaction requires a longer time. The ratiometric assay is able to provide two signals in a measurable window simultaneously and has been widely applied for biosensing applications.[15,16] It affords not only improved sensitivity, but also the built-in self-calibrating capability to eliminate the possible external influence and false signal.[17,18] A DNAzyme is an important molecular tool for the construction of amplified biosensors.[19−21] Due to the predictable manner by Watson−Crick base-pair interactions, the DNAzyme exhibits excellent specificity in molecular recognition.[22] The outstanding catalytic capacity of the DNAzyme benefits the shortening of the reaction time.[23] The basic rule of the DNAzyme-based biosensor is the regulation of stability between a completely hybridized DNAzyme-substrate and cleaved products. Currently, fluorescent DNAzyme biosensors occupy a major place.[24,25]

In this contribution, we have unlocked the potential of an electrochemical DNAzyme biosensor and designed a ratiometric switch for ultrasensitive detection of ctDNA. Methylene blue (MB) and ferrocene (Fc) are selected as two electrochemical species.[26] In the original state, Fc is "on" while MB is "off". Upon recognition of ctDNA, the blocked DNAzyme strand on top of DNA structures at the electrode interface is activated. The subsequently cleaved strand contains a target sequence which in turn initiates the next reaction cycle and leads to the switch of two electrochemical signals. In consequence, the ctDNA biosensor exhibits a good linearity ranging from 100 aM to 100 nM with a quite low limit of detection (LOD) of 25 aM. The results are strong evidence of the great potential of the ctDNA assay in clinical application.

EXPERIMENTAL SECTION

Materials and Chemicals. Tris(2-carboxyethyl)phosphine hydrochloride (TCEP), ethylenediaminetetraacetic acid (EDTA), mercaptohexanol (MCH), and hexaammine-

Received: September 16, 2021
Accepted: January 24, 2022
Published: February 2, 2022

https://doi.org/10.1021/acs.analchem.1c04037
Anal. Chem. 2022, 94, 2779−2784

Scheme 1. Illustration of the Electrochemical Method for the Detection of ctDNA

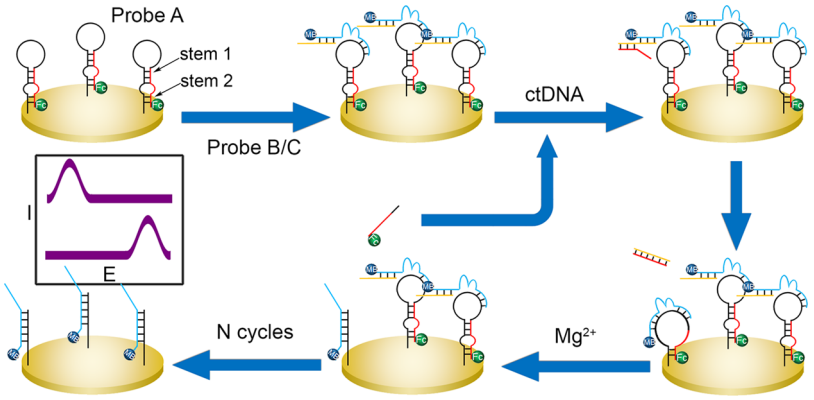

ruthenium(III) chloride ($[Ru(NH_3)_6]^{3+}$) were purchased from Sigma-Aldrich. Calcium chloride, cadmium chloride, magnesium chloride, manganese chloride, and copper nitrate were ordered from Shanghai Aladdin Biochemical Technology Co., Ltd. (Shanghai, China). Human serum samples were supplied by local hospitals (Suzhou, China). All other chemicals were of analytical grade and used as received. Oligonucleotides used in this work were synthesized and purified by Sangon Biotech Co., Ltd. (Shanghai, China). The sequences are listed in Table S1.

Preparation of the Probe A-Modified Electrode. The substrate gold working electrode (diameter: 2 mm) was first incubated with piranha solution (98% H_2SO_4/30% H_2O_2 = 3:1) for 5 min (*Caution: Piranha solution dangerously attacks organic matter!*). After rinsing with double-distilled water, it was carefully polished with silicon carbide paper and alumina powders (1.0, 0.3, 0.05 μm). Subsequently, the gold electrode was sonicated in ethanol and then double-distilled water for 5 min. The treated electrode was further electrochemically cleaned by employing 0.5 M H_2SO_4. Afterward, it was rinsed and then incubated with Probe A (800 nM, 10 mM Tris-HCl, 1 mM EDTA, 10 mM TCEP, and 0.1 M NaCl, pH 7.4) for 8 h at room temperature (about 20 °C). Finally, the electrode was rinsed and treated with MCH for 30 min, which finely modulates the orientation of Probe A for subsequent interactions with Probe B/C.

Recycling Activation of the Blocked DNAzyme. DNA strands were dissolved in 10 mM phosphate-buffered saline (PBS) containing 0.1 M NaCl and 10 mM Mg^{2+} (pH 7.4). Probes B and C with concentrations of 2 μM were blended together. The mixture was heated to 95 °C for 5 min and cooled slowly. The subsequent reactions were conducted at room temperature. The Probe A-modified electrode was incubated with the above solution for 1 h. Afterward, it was further treated with various concentrations of the target DNA (diluted with PBS) for 1 h and then 35 mM Mg^{2+} for another 1 h.

Electrochemical Measurements. All electrochemical measurements were carried out with a CHI 660D electrochemical workstation (CH Instrument, China). A three-electrode system was assembled including a platinum auxiliary electrode, a saturated calomel reference electrode, and the DNA-modified gold electrode as the working electrode. Cyclic voltammetry (CV) was carried out from 0.55 to −0.2 V with a scan rate of 50 mV s^{-1}. Electrochemical impedance spectroscopy (EIS) was carried out with the parameters as follows: a biasing potential, 0.215 V; amplitude, 5 mV; and frequency range, 0.1 Hz to 100 kHz. Both CV and EIS measurements were performed in the electrolyte of 5 mM $[Fe(CN)_6]^{3-/4-}$ with 1 M KNO_3. Chronocoulometry (CC) was performed in the electrolyte of 10 mM Tris-HCl solutions (pH 7.4) containing 50 μM $[Ru(NH_3)_6]^{3+}$. Square wave voltammetry (SWV) was performed in 20 mM Tris-HCl (pH 7.45). The parameters included a 25 mV amplitude signal, 4 mV step potential, 50 Hz frequency, and scan range of 0.6 to −0.6 V.

Electrophoresis Measurements. Polyacrylamide gel electrophoresis was carried out in the Tris-boric acid buffer solution (90 mM, 1 mM EDTA, pH 8.0) at 120 V for 40 min. Subsequently, the obtained polyacrylamide gel was stained with 4S Red Plus, which was further photographed under UV light using a Gel DocTM XR+ Imaging System (Bio-Rad).

RESULTS AND DISCUSSION

Sensing Principle. The detailed working mechanism of the method is illustrated in Scheme 1. A hairpin-structured DNA Probe A, DNAzyme-embodied Probe B, and recognizing strand of Probe C are designed.[27] Briefly, Probe A is modified on the gold electrode via sulfur−gold chemistry, which is first studied by chronocoulometry. The redox charge of $[Ru(NH_3)_6]^{3+}$ adsorbed on Probe A can be revealed by the chronocoulometric intercept. After the modification of Probe A (800 nM), the intercept increases, indicating successful immobilization (Figure S1A). According to the Cottrell equation, the density of Probe A at the surface of the electrode is calculated to be about 1.68 pmol cm^{-2}. Due to the 3′ terminal Fc of Probe A, a significant electrochemical response can be recorded. A scissile ribonucleic acid adenosine (rA) site is positioned on top of the loop region of Probe A and a bubble is designed in the stem section that divides it into two parts. Probe B contains a Mg^{2+}-dependent DNAzyme sequence, which is labeled with MB at the 3′ terminal. It is able to open stem 1 of Probe A, resulting in the formation of a larger loop. By introducing the cofactor of Mg^{2+}, the substrate strand can be cleaved at the site of rA. However, the complete interaction between Probes A and B can be inhibited by Probe C. The DNA composites of Probes A, B, and C are assembled with the blocked DNAzyme at the initial stage. After the introduction of ctDNA, a more stable duplex (ctDNA/Probe C) is formed by the strand displacement reaction, which shows a higher melting temperature (T_m). In the absence of the locking strand of Probe C, the single-stranded arm of the DNAzyme in Probe B is released, which further anchors in Probe A. In addition, DNAzyme is activated and catalyzes the cleavage of Probe A in the presence of cofactor Mg^{2+}.

https://doi.org/10.1021/acs.analchem.1c04037
Anal. Chem. 2022, 94, 2779−2784

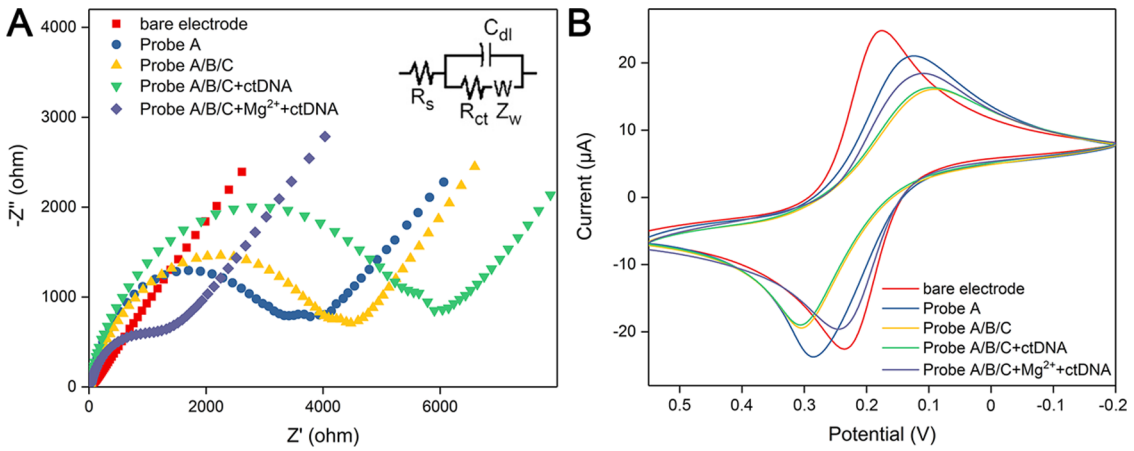

Figure 1. (A) Nyquist plots and (B) cyclic voltammograms corresponding to the bare electrode, Probe A (0.8 μM)-modified electrode, and after hybridization with Probe B/C (1 μM) in the absence and presence of ctDNA (1 nM) and Mg^{2+} (35 mM), respectively. The inset shows the electrical equivalent circuit.

Subsequently, stem 2 is disassociated and half of Probe A containing Fc is released in the solution. On the contrary, MB at the Probe B terminal is located close to the electrode surface. Therefore, an electrochemical switch is achieved (MB and Fc signals). In addition, the cleaved part of Probe A contains the sequence of the target ctDNA, which is able to activate other blocked DNAzymes, resulting in recycled transformation of DNA structures and variations of the two electrochemical species. This enzyme-free amplification induces ratiometric signal accumulation, which benefits the improvement of sensitivity toward ctDNA analysis. T_m values of double-stranded regions during the recycled reactions have been calculated, which theoretically demonstrate thermodynamical favorability from the initial stage to the final stage (Figure S1B). Polyacrylamide gel electrophoresis is also performed to characterize the sizes of reactants and products throughout the reaction, further confirming the feasibility of the proposed strategy. Lanes B and C represent Probes B and C, respectively. After hybridization, the partial duplex of Probes B and C is evidenced by a new band with a larger molecular weight in lane D. After the interaction between Probe A and Probe B/C, a band with an even larger molecular weight is observed, which is ascribed to the complex of Probe A/B/C (lane E and F). The further introduction of the target displaces Probe C, leading to the formation of another duplex and Probe A/B complex. Both of the products can be found in lane G. In addition, since Probe A/B/C is consumed, the corresponding band disappears. Finally, in the presence of the cofactor of Mg^{2+}, the DNAzyme is activated to cleave Probe A and the emerged new bands are the reaction products (Figure S2).

Electrochemical Characterization of the Sensing Interface. EIS and CV are first performed to probe the reaction processes occurring at the electrode surface. As shown in Figure 1A, a straight line is observed for the Nyquist plot of the bare electrode, demonstrating excellent conductivity of the substrate gold electrode. After being modified with Probe A, the DNA layer repels the negatively charged electrochemical species and leads to a large charge transfer resistance (R_{ct}), which is reflected by the increased semicircle domain of the plot. After further interaction with the duplex of Probe B/C, the semicircle domain is enlarged correspondingly. The further employed ctDNA is able to trigger the conformation change of the DNA structure. Although Probe C is displaced, a more compact DNA structure is formed, which contributes to the increased R_{ct} and the semicircle domain is even larger. However, the further addition of Mg^{2+} assists the cleavage reaction catalyzed by the DNAzyme. Since a recycling mechanism is involved, a large number of Probe A is cleaved. Therefore, the semicircle domain of the Nyquist plot decreases remarkably. EIS results are quite consistent with the reaction process. A similar trend can be observed in CV. The intensity of the pair of well-defined current peaks is the reflection of the charge transfer resistance. As shown in Figure 1B, with the procedure of DNA structure transformation, the changes of peaks are consistent with the variation of R_{ct} values in Figure 1A.

To monitor the electrochemical responses of MB and Fc, SWV is conducted. As illustrated in Figure 2, without the modification of DNA, a flat curve is obtained for the bare electrode. The successful immobilization of Probe A positions a larger number of Fc near the electrode surface, thus, a

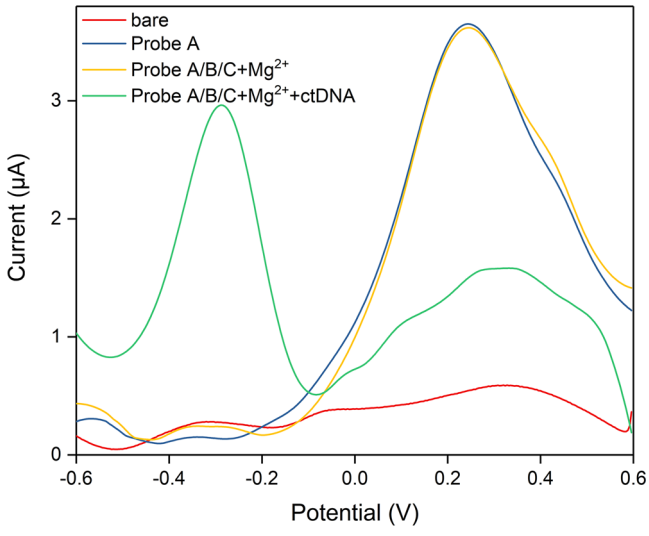

Figure 2. Square wave voltammograms of the bare electrode, Probe A (0.8 μM)-modified electrode, and after hybridization with Probe B/C (1 μM) in the absence and presence of ctDNA (1 nM). The curves are baseline corrected.

https://doi.org/10.1021/acs.analchem.1c04037
Anal. Chem. 2022, 94, 2779−2784

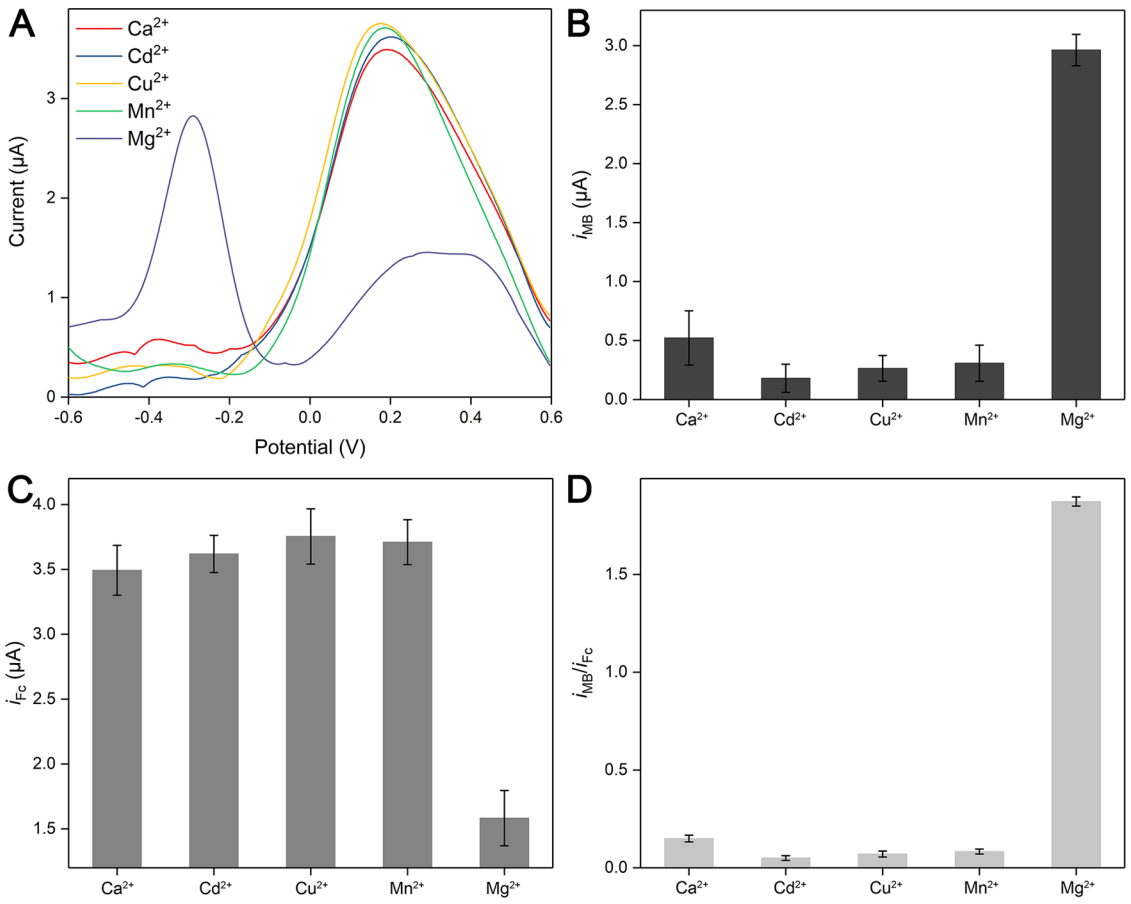

Figure 3. (A) Square wave voltammograms of the Probe A/B/C-modified electrode after the DNAzyme-catalyzed reaction with Ca^{2+}, Cd^{2+}, Cu^{2+}, Mn^{2+}, and Mg^{2+}, respectively. (B) Peak currents of MB, (C) peak currents of Fc, and (D) their ratios in the cases of Ca^{2+}, Cd^{2+}, Cu^{2+}, Mn^{2+}, and Mg^{2+}. The concentrations of these ions are 35 mM. The curves are baseline corrected.

significant peak around 0.3 V appears. After further introduction of Probes B and C, the Fc peak barely changes, and a slight peak around −0.3 V emerges, which is ascribed to MB at the 3′ terminal of Probe B. The large distance between MB and the electrode surface leads to the limited intensity of the peak. After ctDNA initiated activation of the DNAzyme and recycling cleavage reactions, Probe A is cleaved and the moiety with Fc is kept away from the electrode. Meanwhile, Probe B is hybridized with the other part of Probe A, and MB is located near the electrode. As a result, the Fc peak decreases, while the MB peak increases. Since the distance between the current peaks of MB and Fc in the electrochemical window is quite large, the responses could be distinguished independently without interference. By analyzing the two peak intensities simultaneously, the reliability and sensitivity for the analysis of ctDNA can be improved.

Electrochemical Quantification. To achieve the best analytical performances, several important experimental conditions should be optimized. First, the density of Probe A determines the intensity of the initial Fc. We have prepared various concentrations of Probe A for the incubation of the electrode. With the increase of Probe A, the semicircle domain of the Nyquist plot of the electrode is increased, which implies the increased density of the Probe A monolayer on the electrode. More directly, the Fc signal reflected in the square wave voltammogram also increases with a larger Probe A concentration. The intensities of R_{ct} for EIS and the peak current for SWV (Fc) increase with the Probe A concentration from 100 to 800 nM. However, in the presence of more Probe A, the interface might be too crowded and the modification is not as effective as 800 nM Probe A incubation, which is reflected by the slight drops of R_{ct} and the SWV peak current. Thus, we choose 800 nM as the optimal value for the Probe A concentration (Figure S3). We have then studied the accuracy and reproducibility of the DNA-modified electrode. The Fc response of one electrode is tested after repeated DNA modifications and cleaning treatments, which barely change after five cycles (Figure S4A). We have also compared the Fc response of Probe A modification on independent electrodes, the results of which are identical (Figure S4B). On the other hand, the activation of the DNAzyme and cleavage reaction is the core of the biosensor. We have prepared various concentrations of Mg^{2+} to participate in the reaction and took $i_{MB}-i_{Fc}$ as the indicator. In addition, different reaction times of DNAzyme cleavage in the presence of Mg^{2+} are also evaluated. By comparing the ratiometric electrochemical responses, 35 mM Mg^{2+} and the 60 min cleavage reaction time are chosen for quantitative analysis of the target ctDNA (Figure S5).

In this study, enzyme-free amplification is developed, which improves the practical utility of the system. To confirm the activity of the cofactor-specific DNAzyme, we have checked other potential ions including Ca^{2+}, Cd^{2+}, Cu^{2+}, and Mn^{2+}. As shown in Figure 3A, in the cases of these ions, MB peaks are negligible, while Fc peaks are nearly unchanged. The detailed comparisons listed in Figure 3B−D demonstrate that the

https://doi.org/10.1021/acs.analchem.1c04037
Anal. Chem. 2022, 94, 2779−2784

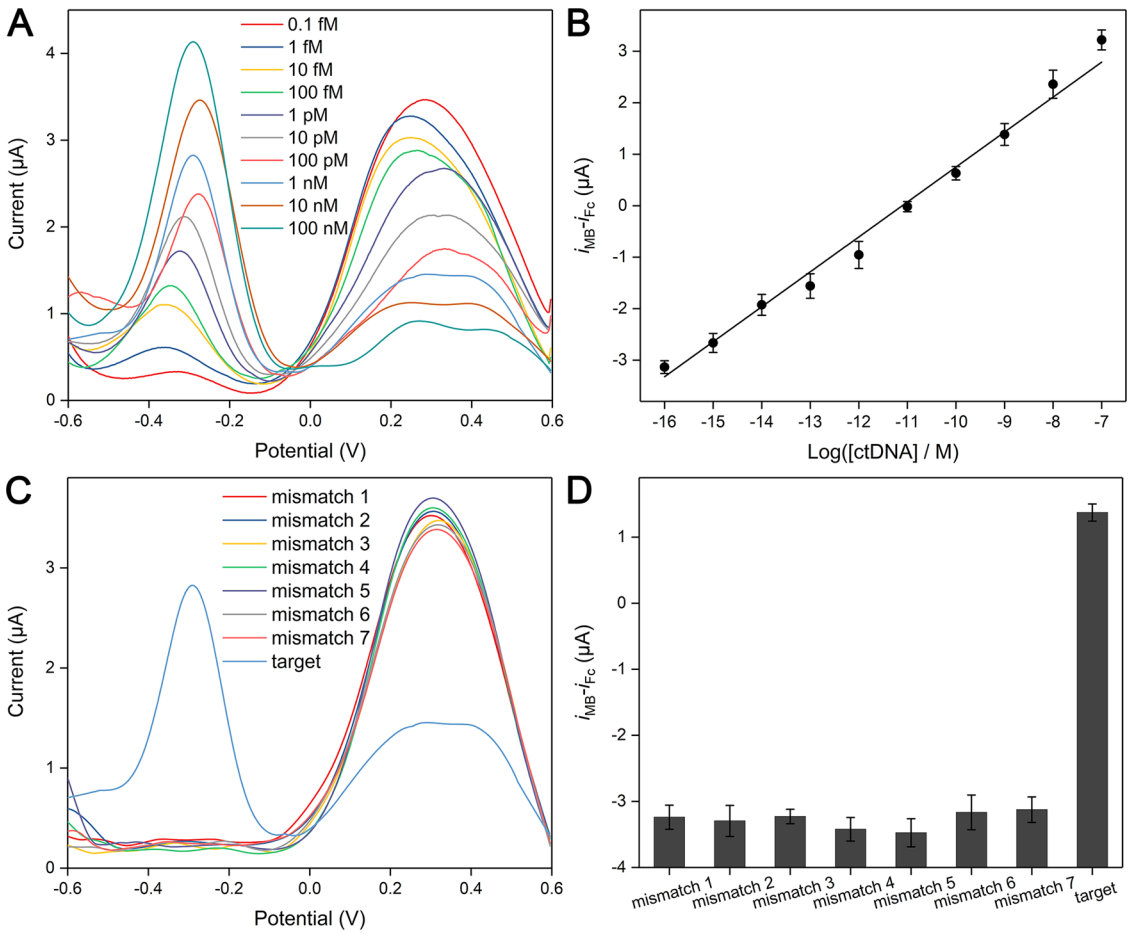

Figure 4. (A) Square wave voltammograms for the detection of ctDNA with the concentrations of 10^{-16}, 10^{-15}, 10^{-14}, 10^{-13}, 10^{-12}, 10^{-11}, 10^{-10}, 10^{-9}, 10^{-8}, and 10^{-7} M. (B) Calibration curve reflecting the relationship between ctDNA concentrations and peak differences between MB and Fc. (C) Square wave voltammograms for the detection of ctDNA (1 nM) and mismatched sequences (1 nM). (D) Corresponding peak differences. The curves are baseline corrected.

applied DNAzyme is sensitive to Mg^{2+} and the interference by other divalent ions in the system is limited. We have then measured SWV curves in the presence of various concentrations of target ctDNA (Figure 4A). It is clearly shown that with a larger amount of ctDNA, the MB peak gradually increases, while the Fc peak decreases correspondingly. A detailed relationship between the difference of the two peaks and logarithmic ctDNA concentration is established in Figure 4B. A wide linear range is obtained from 100 aM to 100 nM. The equation is

$$y = 7.540 + 0.679x (n = 3,\ R^2 = 0.990)$$

in which y is the difference between the peaks of MB and Fc, and x is the logarithmic ctDNA concentration. The wide linear range is mainly ascribed to the large electroactive area to support the DNA probes.[28] The limit of detection (LOD) is calculated to be 25 aM, which is quite low. The ultrahigh sensitivity is achieved by the DNAzyme-catalyzed reaction, self-calibrating capability of the ratiometric assay, and recycles of target and cleaved products. Compared with some representative nucleic acid assays developed previously, this study shows sufficient superiority (Table S2). The reproducibility of this biosensor is evaluated by testing eight measurements of five independent concentrations of ctDNA. The relative standard deviation (RSD) is less than 5%, suggesting excellent reproducibility.

Investigations of Selectivity and Practical Utility. We have further verified the specificity of this biosensor by introducing seven mismatched sequences compared with the target ctDNA. As shown in Figure 4C, none of these sequences can result in obvious changes of Fc and MB peaks. A detailed peak intensity comparison in Figure 4D clearly demonstrates the high selectivity of the proposed method. To confirm the proof-of-concept of clinical application, we have performed recovery experiments by spiking different levels of ctDNA into human serum samples. After challenging these samples with the proposed electrochemical method, the concentrations of ctDNA are calculated by analyzing the measured peaks. The obtained values are in good agreement with the spiked values. The RSD is from 2.8 to 5.5% and the recovery is in the range of 97−108.3% (Table S3). In addition, to simplify operations, Mg^{2+} could be directly spiked in the samples, integrating target recognition and cleavage cycles. Great potential is confirmed for the method to be utilized in actual biological sample detection.

CONCLUSIONS

In summary, this study fabricates a novel ratiometric electrochemical sensing strategy for the analysis of ctDNA based on DNAzyme-mediated cleavage reaction coupled with recycling activation. With the specially designed hairpin-structured Probe A with a bubble and partial-complementary

https://doi.org/10.1021/acs.analchem.1c04037
Anal. Chem. 2022, 94, 2779−2784

Probe B/C, we could rapidly identify the target ctDNA. In addition, with the amplification by recycled activation of the DNAzyme, ultrahigh sensitivity is achieved with a LOD as low as 25 aM. The high selectivity is confirmed by challenging mismatched DNA strands, and the results of serum sample assays are in agreement with spiked values. It is regarded as a promising biosensor for rapid, simple, precise, and ultrasensitive analysis of ctDNA.

■ ASSOCIATED CONTENT

Supporting Information

The Supporting Information is available free of charge at https://pubs.acs.org/doi/10.1021/acs.analchem.1c04037.

Chronocoulometry curves of a DNA-modified electrode; T_m values; polyacrylamide gel electrophoresis analysis of the reaction process; EIS and SWV optimizations of the Probe A concentration, Mg^{2+} concentration, and reaction time; reproducibility investigation; DNA and RNA sequences; comparison of analytical performances; and serum sample detection performances (PDF)

■ AUTHOR INFORMATION

Corresponding Author

Peng Miao − *University of Science and Technology of China, Hefei 230026, China; Suzhou Institute of Biomedical Engineering and Technology, Chinese Academy of Sciences, Suzhou 215163, China;* orcid.org/0000-0003-3993-4778; Phone: +86-512-69588279; Email: miaopeng@sibet.ac.cn

Authors

Hua Chai − *University of Science and Technology of China, Hefei 230026, China; Suzhou Institute of Biomedical Engineering and Technology, Chinese Academy of Sciences, Suzhou 215163, China*

Yuguo Tang − *Suzhou Institute of Biomedical Engineering and Technology, Chinese Academy of Sciences, Suzhou 215163, China*

Zhenzhen Guo − *Suzhou Institute of Biomedical Engineering and Technology, Chinese Academy of Sciences, Suzhou 215163, China; Ji Hua Laboratory, Foshan 528200, China*

Complete contact information is available at: https://pubs.acs.org/10.1021/acs.analchem.1c04037

Author Contributions

All authors have given approval to the final version of the manuscript.

Notes

The authors declare no competing financial interest.

■ ACKNOWLEDGMENTS

This work is supported by the Science and Technology Cooperation Project between the Chinese and Australian Governments (Grant No. 2017YFE0132300), the Science and Technology Project of Ji Hua Laboratory (Grant No. X190191TD190), and the Natural Science Foundation of Jiangsu Province (Grant No. BK20201184).

■ REFERENCES

(1) Newman, A. M.; Lovejoy, A. F.; Klass, D. M.; Kurtz, D. M.; Chabon, J. J.; Scherer, F.; Stehr, H.; Liu, C. L.; Bratman, S. V.; Say, C.; Zhou, L.; Carter, J. N.; West, R. B.; Sledge, G. W., Jr.; Shrager, J. B.; Loo, B. W.; Neal, J. W.; Wakelee, H. A.; Diehn, M.; Alizadeh, A. A. *Nat. Biotechnol.* **2016**, *34*, 547−555.

(2) Thierry, A. R.; Mouliere, F.; El Messaoudi, S.; Mollevi, C.; Lopez-Crapez, E.; Rolet, F.; Gillet, B.; Gongora, C.; Dechelotte, P.; Robert, B.; Del Rio, M.; Lamy, P.-J.; Bibeau, F.; Nouaille, M.; Loriot, V.; Jarrousse, A.-S.; Molina, F.; Mathonnet, M.; Pezet, D.; Ychou, M. *Nat. Med.* **2014**, *20*, 430−435.

(3) Zhu, G.; Guo, Y. A.; Ho, D.; Poon, P.; Poh, Z. W.; Wong, P. M.; Gan, A.; Chang, M. M.; Kleftogiannis, D.; Lau, Y. T.; Tay, B.; Lim, W. J.; Chua, C.; Tan, T. J.; Koo, S.-L.; Chong, D. Q.; Yap, Y. S.; Tan, I.; Ng, S.; Skanderup, A. J. *Nat. Commun.* **2021**, *12*, No. 2229.

(4) Newman, A. M.; Bratman, S. V.; To, J.; Wynne, J. F.; Eclov, N. C. W.; Modlin, L. A.; Liu, C. L.; Neal, J. W.; Wakelee, H. A.; Merritt, R. E.; Shrager, J. B.; Loo, B. W.; Alizadeh, A. A.; Diehn, M. *Nat. Med.* **2014**, *20*, 548−554.

(5) Moding, E. J.; Liu, Y.; Nabet, B. Y.; Chabon, J. J.; Chaudhuri, A. A.; Hui, A. B.; Bonilla, R. F.; Ko, R. B.; Yoo, C. H.; Gojenola, L.; Jones, C. D.; He, J.; Qiao, Y.; Xu, T.; Heymach, J. V.; Tsao, A.; Liao, Z.; Gomez, D. R.; Das, M.; Padda, S. K.; Ramchandran, K. J.; Neal, J. W.; Wakelee, H. A.; Loo, B. W.; Lin, S. H.; Alizadeh, A. A.; Diehn, M. *Nat. Cancer* **2020**, *1*, 176−183.

(6) Hu, P.; Zhang, S.; Wu, T.; Ni, D.; Fan, W.; Zhu, Y.; Qian, R.; Shi, J. *Adv. Mater.* **2018**, *30*, No. 1801690.

(7) Chai, H.; Miao, P. *Chin. Chem. Lett.* **2021**, *32*, 783−786.

(8) Wang, Y.; Kong, S. L.; Su, X. D. *RSC Adv.* **2020**, *10*, 1476−1483.

(9) Chen, D.; Wu, Y.; Hoque, S.; Tilley, R. D.; Gooding, J. J. *Chem. Sci.* **2021**, *12*, 5196−5201.

(10) Wang, Y.; Kong, S. L.; Su, X. *Chem. Commun.* **2021**, *57*, 6796−6799.

(11) Chen, C.; He, R.; Zhang, Z.; Chen, Y. *Analyst* **2020**, *145*, 7603−7608.

(12) Ou, C.-Y.; Vu, T.; Grunwald, J. T.; Toledano, M.; Zimak, J.; Toosky, M.; Shen, B.; Zell, J. A.; Gratton, E.; Abram, T. J.; Zhao, W. *Lab Chip* **2019**, *19*, 993−1005.

(13) Gao, F.; Chu, Y.; Ai, Y.; Yang, W.; Lin, Z.; Wang, Q. *Chin. Chem. Lett.* **2021**, *32*, 2192−2196.

(14) Zhang, J.; Lao, R.; Song, S.; Yan, Z.; Fan, C. *Anal. Chem.* **2008**, *80*, 9029−9033.

(15) Wu, X.; Lu, Y.; Liu, B.; Chen, Y.; Zhang, J.; Zhou, Y. *Chin. Chem. Lett.* **2021**, *32*, 2380−2384.

(16) Deng, C.; Pi, X.; Qian, P.; Chen, X.; Wu, W.; Xiang, J. *Anal. Chem.* **2017**, *89*, 966−973.

(17) Ma, Y.; Xu, L.; Yin, B.; Shang, J.; Chen, F.; Xu, J.; Song, Z. L.; Nan, B.; Song, G.; Zhang, X. B. *Nano Lett.* **2021**, *21*, 4484−4493.

(18) Liu, J. W.; Luo, Y.; Wang, Y. M.; Duan, L. Y.; Jiang, J. H.; Yu, R. Q. *ACS Appl. Mater. Interfaces* **2016**, *8*, 33439−33445.

(19) Jia, Y.; Chen, L.; Liu, J.; Li, W.; Gu, H. *Chem* **2021**, *7*, 959−981.

(20) Zhang, C.; Yang, J.; Jiang, S.; Liu, Y.; Yan, H. *Nano Lett.* **2016**, *16*, 736−741.

(21) Shan, Z.; Lyu, M.; Curry, D.; Oakley, D.; Oakes, K.; Zhang, X. *Chin. Chem. Lett.* **2019**, *30*, 1652−1654.

(22) Wang, J.; Wang, H.; Wang, H.; He, S.; Li, R.; Deng, Z.; Liu, X.; Wang, F. *ACS Nano* **2019**, *13*, 5852−5863.

(23) Hou, M.; Yin, X.; Jiang, J.; He, J. *ACS Appl. Mater. Interfaces* **2021**, *13*, 15031−15039.

(24) Sorrentino, D.; Ranallo, S.; Ricci, F. *ACS Appl. Mater. Interfaces* **2021**, *13*, 9300−9305.

(25) Wang, L.; Zhou, H.; Liu, B.; Zhao, C.; Fan, J.; Wang, W.; Tong, C. *Anal. Chem.* **2017**, *89*, 11014−11020.

(26) Lu, N.; Pei, H.; Ge, Z.; Simmons, C. R.; Yan, H.; Fan, C. *J. Am. Chem. Soc.* **2012**, *134*, 13148−13151.

(27) Xue, C.; Luo, M.; Wang, L.; Li, C.; Hu, S.; Yu, X.; Yuan, P.; Wu, Z.-S. *Anal. Chem.* **2021**, *93*, 9869−9877.

(28) Lin, D. H.; Pillai, R. G.; Lee, W. E.; Jemere, A. B. *Microchim. Acta* **2019**, *186*, No. 169.